

Photochemically Driven Collapse of Titan's Atmosphere

Ralph D. Lorenz,* Christopher P. McKay, Jonathan I. Lunine

Saturn's giant moon Titan has a thick (1.5 bar) nitrogen atmosphere, which has a temperature structure that is controlled by the absorption of solar and thermal radiation by methane, hydrogen, and organic aerosols into which methane is irreversibly converted by photolysis. Previous studies of Titan's climate evolution have been done with the assumption that the methane abundance was maintained against photolytic depletion throughout Titan's history, either by continuous supply from the interior or by buffering by a surface or near surface reservoir. Radiative-convective and radiative-saturated equilibrium models of Titan's atmosphere show that methane depletion may have allowed Titan's atmosphere to cool so that nitrogen, its main constituent, condenses onto the surface, collapsing Titan into a Triton-like frozen state with a thin atmosphere.

Titan's present surface temperature differs from its effective temperature (1) because of the competing influences of a strong greenhouse effect (2) dominated by the collision-induced absorption of N_2 , methane (CH_4), and H_2 in infrared (IR) wavelengths (especially CH_4 - N_2 opacity in the 200 to 600 cm^{-1} window region) and a comparable antigreenhouse effect that is due to absorption of sunlight by haze and CH_4 in the upper atmosphere (3). The haze and H_2 ultimately depend on the photolysis of CH_4 (4), which in turn is assumed to be continuously resupplied. Previous studies (5, 6) were done with the assumption that a reservoir of CH_4 existed at the surface. If CH_4 resupply lagged behind its destruction, as might be expected if CH_4 delivery to the surface (7) was episodic on time scales longer than its photochemical lifetime [1 to 10 million years (4)], then the CH_4 abundance, and consequently the surface temperature, would fall (8).

Once the CH_4 concentration has decreased, the production of photochemical haze and H_2 slows. The typical residence time of stratospheric haze particles is ~ 1000 years (9). Once the haze falls out, surface temperatures increase to about 88 K because reduced haze opacity allows more solar radiation to reach the surface. However, the atmospheric structure changes profoundly. Present stratospheric temperatures are maintained at ~ 180 K as a result of absorption of solar radiation by the haze—without the haze present, stratospheric temperatures would decrease to below 60 K (10).

The final effect of CH_4 depletion is the

loss of H_2 . H_2 participates little in atmospheric chemistry once it is produced, and its abundance is balanced between photochemical production and escape to space. Once photochemical production ceases, the abundance decreases slowly [with an escape time of ~ 2 million years (11)]. Despite its low abundance, H_2 is an important greenhouse gas, providing, along with N_2 , most of the opacity above 600 cm^{-1} . After the H_2

has escaped, the surface temperature again decreases, down to about 86 K, slightly above the equilibrium temperature, because of the slight greenhouse effect resulting from the N_2 opacity below (longward of) 200 cm^{-1} .

These calculations assume the present solar constant of $15.6 W m^{-2}$ and a surface albedo of 0.2 and ignore the effects of N_2 condensation. As noted in earlier studies (5), when the atmosphere cools during the CH_4 depletion, the model temperature at some altitudes in the atmosphere (here, at ~ 10 km for 20% CH_4 surface humidity) becomes lower than the saturation temperature of N_2 . Nitrogen clouds would therefore form at this point. However, a model of cloud droplet growth and descent rates (12) suggests that drops would grow and fall rapidly: When realistic constraints on the flux of latent heat (13) associated with clouds, and the number of cloud condensation nuclei, are invoked, we find that the total column optical depth associated with N_2 clouds is small ($\tau < 0.1$). Thus, although condensation affects the temperature profile by a latent heat flux (14), the radiative effects of N_2 clouds can be ignored.

When the atmosphere is cooler still as a

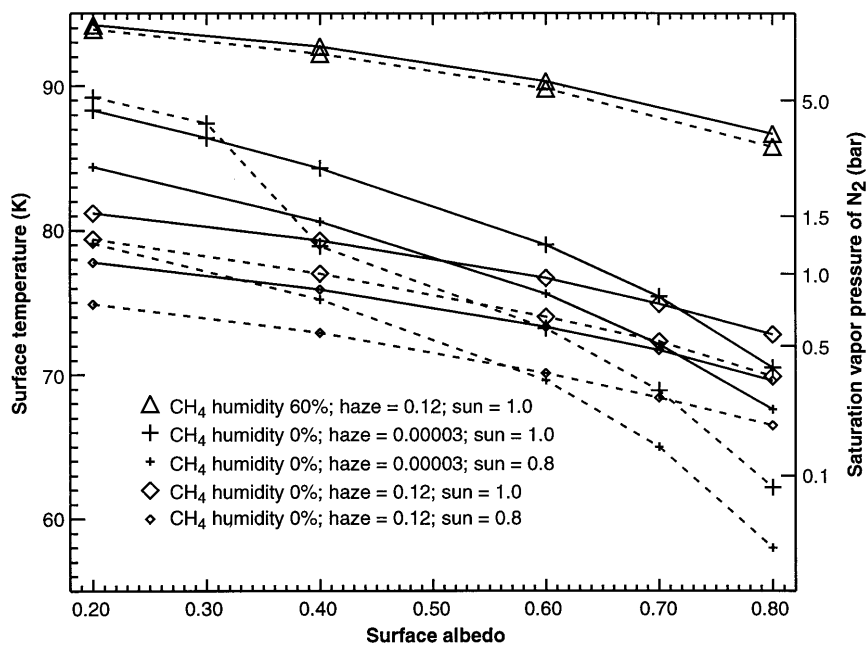


Fig. 1. Titan surface temperatures. The present surface temperature of 94 K is consistent with a CH_4 surface relative humidity of $\sim 60\%$ (triangles), a haze production of 0.12 (in units of $10^{-14} g cm^{-1} s^{-1}$), and a surface albedo of 0.4 or lower. The solid lines indicate the radiative-convective model (3) and the dashed lines the radiative-saturated model (74). The strong absorption of sunlight by the haze makes the surface temperature relatively insensitive to surface visible albedo. Removing the CH_4 (diamonds) drops the temperature by 12 to 14 K. Where surface temperatures are below the saturation temperature of the present 1.5 bar of N_2 , the saturated model predicts somewhat lower temperatures. Reducing the haze production rate to an arbitrarily small value (crosses) increases low-albedo surface temperatures but decreases high-albedo temperatures. Curves are given for solar luminosities of 100 and 80% of the present value. Hydrogen is assumed present at 0.001 mole fraction for all cases; its removal decreases the temperature by a few kelvin. The departure of the saturated model from the radiative-convective one indicates the onset of condensation.

R. D. Lorenz and J. I. Lunine, Department of Planetary Sciences, Lunar and Planetary Laboratory, University of Arizona, Tucson, AZ 85721, USA.
C. P. McKay, NASA Ames Research Center, Moffett Field, CA 94035, USA.

*To whom correspondence should be addressed. E-mail: rlorenz@lpl.arizona.edu

result of lower CH₄ abundances or a lower solar constant (3 billion years ago the latter was 0.8 times the present value) or both, saturation extends down to the surface and liquid N₂ can accumulate there. Rainout of hundreds of millibar of N₂ (corresponding to tens of meters of liquid depth) might affect the surface albedo [CH₄ rainfall on elevated terrain has been proposed (15, 16) to maintain the high albedo of a bright region identified on Titan's surface in Hubble Space Telescope images (16)]. The present surface albedo (17) at 10,000 cm⁻¹ (the shortest wavelength measured to date) ranges from 0.29 to 0.47 (the hemisphere containing the bright region). In comparison, albedos elsewhere in the saturnian system (18) are typically 0.5 or higher. The effects of varying surface albedo and CH₄ depletion are shown in Fig. 1.

Liquid N₂ itself is not radiatively active at visible wavelengths, so seas formed by N₂ condensation will reflect the albedo of the seabed or suspended particulates or both. However, downslope transport of dark material (15) that concentrates it in basins (for example, craters) may cause an increase in the global average albedo. Loss of N₂ from the atmosphere also causes cooling by a decrease in N₂-N₂ collision-induced opacity below 200 cm⁻¹. However, as the surface temperature drops, the outgoing thermal radiation is shifted to longer wavelengths where the residual N₂ opacity becomes more important, producing a stabilizing effect. Earlier calculations (8) revealed that scaling Triton's surface temperatures with insolation at Titan's distance from the sun yields temperatures above the N₂ freezing point (63 K, at which its vapor pressure is 0.1 bar). Thus, on the basis of globally averaged models it would be unlikely that Titan's atmosphere would completely freeze out.

Such models ignore equator-to-pole temperature contrasts at the surface, which are small at present, due mostly to meridional heat transport by the massive atmosphere. Consider that a global average temperature of 65 K might represent an equator-to-pole temperature range of 60 to 70 K. The difference in radiative flux (σT^4 , with σ the Stefan-Boltzmann constant $5.67 \times 10^{-8} \text{ W m}^{-2} \text{ K}^{-4}$ and T is temperature) between 70 and 60 K is about 1 W m^{-2} ; to make this up from lower latitudes requires advective heat transport of about 1 MW m^{-1} across a line of latitude. If the atmospheric pressure should fall significantly, meridional heat transport by advection (19) may become inhibited, assuming that the role of meridional winds is not taken up by equator-to-pole motions in the $\sim 100\text{-m}$ layer of liquid N₂ deposited onto the surface (20). In this case, polar temperatures could

decrease, atmospheric pressure (controlled by the vapor pressure of N₂ at Titan's cold-est point) could decrease further, and bright N₂ frost would form at the poles. Once in a cooler state, reintroduction of CH₄ to the surface by volcanism may not immediately reverse the evolution sketched above. If the surface is cold, CH₄ vapor pressures will be too low to enable a radiatively significant amount of gas (~ 10 mbar) to form. However, unless resurfacing by frost deposition is rapid, solar ultraviolet or energetic particle bombardment (or both) would darken bright CH₄ deposits, warming them. This process, with the secular increase in solar luminosity, ensures the eventual reinflation of the atmosphere from a frozen state. Once the surface warms a little, low-latitude N₂ would volatilize, and increased heat transport to high latitudes would reevaporate polar reservoirs of N₂ in a positive feedback (21). Reinflation from a warmer N₂ sea surface state (surface pressure of 100 to 1400 mbar) would be gradual, as CH₄ would dissolve in the N₂ (22) and its vapor pressure would remain low. Once reinflation began (either by secular warming, or perhaps by a thermal or impact event) the positive feedback would return the atmosphere to near its present state.

Whether these collapse and reinflation processes have occurred on Titan remains uncertain. However, atmospheric collapse and condensation at the poles might leave observable morphological clues, such as U-shaped valleys near the poles as a result of glacial erosion (15), a small-crater population inconsistent with present-day atmospheric shielding (23), or evidence of cryoclastic volcanism that is inhibited by the present atmospheric pressure (24). Even if complete freezeout to tens of millibar never occurred, a collapse to a 100-mbar state with seas of liquid N₂ would have been a cataclysmic event. It is sobering that the only significant N₂ atmosphere in the solar system apart from our own may have had such a precarious history.

REFERENCES AND NOTES

1. The effective temperature is that temperature at which a black body would emit the total solar radiation absorbed by Titan. The temperature is estimated at 82 K at present (3).
2. C. P. McKay, J. B. Pollack, and R. Courtin [*Science* **253**, 1118 (1991)] described the haze greenhouse and anti-greenhouse effects. R. E. Samuelson [*Icarus* **53**, 364 (1983)] presented an analytic model illustrating stratospheric heating by haze absorption and greenhouse warming by tropospheric IR opacity.
3. C. P. McKay, J. B. Pollack, R. Courtin, *Icarus* **80**, 23 (1989).
4. Y. L. Yung, M. Allen, J. P. Pinto, *Astrophys. J. Suppl. Ser.* **55**, 465 (1984); D. Toubanc *et al.*, *Icarus* **113**, 2 (1995); L. M. Lara, R. D. Lorenz, R. Rodrigo, *Planet. Space Sci.* **42**, 5 (1994).
5. C. P. McKay, J. I. Lunine, R. Courtin, *Icarus* **102**, 88 (1993).

6. J. I. Lunine and B. Rizk, *ibid.* **80**, 370 (1989). N. Dubouloz, F. Raulin, E. Lellouch, and D. Gautier [*ibid.* **82**, 81 (1989)] examined the equilibrium composition of such a liquid reservoir with the present atmosphere.
7. When CH₄ is delivered to the surface it may do so in sufficient abundance to form CH₄ seas and lakes, even if no such deposits are present now. Certainly, remote sensing data [for example, D. O. Muhleman, A. W. Grossman, B. J. Butler, M. A. Slade, *Science* **248**, 975 (1990)] rule out global hydrocarbon deposits deeper than a few tens of meters.
8. R. D. Lorenz, J. I. Lunine, J. A. Grier, M. Fisher, *J. Geophys. Res.* **100**, 26377 (1995).
9. O. B. Toon *et al.*, *Icarus* **95**, 24 (1992). To first order, a constant photolysis rate gives a constant reduction with time of the CH₄ relative humidity. As the temperature decreases and the vapor pressure of CH₄ decreases, the decrease in relative humidity slows a little. Methane delivery from the troposphere to the stratosphere, where it is destroyed, may be limited by a cold-trap near the tropopause, further slowing depletion. The exact temperature trajectory also depends on the production and loss of haze and H₂: Because at present CH₄ photolysis is photon-limited rather than CH₄-limited, CH₄ depletion is probably near total before the haze and hydrogen production is significantly affected, hence our "sequential" treatment of CH₄, haze, and H₂ depletion. Note that Triton has a very low CH₄ atmospheric abundance, yet it still has a photochemical haze, although one that is about 1000 times optically thinner than Titan's present one.
10. Our model does not include all the minor opacity sources that may be present, so exactly how cold the stratosphere gets cannot be stated with certainty.
11. J. L. Bertaux and G. Kockarts, *J. Geophys. Res.* **88**, 8716 (1983).
12. R. D. Lorenz [*Planet. Space Sci.* **41**, 647 (1993)] showed that CH₄ raindrops in the present atmosphere can grow to about 9 mm in diameter before aerodynamic forces overcome surface tension and tear the drops apart. Drops fall at about 2 m s^{-1} at most. Nitrogen drops are somewhat denser and can fall slightly faster. However, the time for a drop to grow to a few millimeters in diameter is short compared with the time (~ 1 hour) for such a drop to fall a kilometer or two.
13. Clearly, the product $NVML$ (with N the number of drops per unit area, V their descent speed, M the drop mass, and L the latent heat of evaporation) must be lower than the available insolation (3.7 W m^{-2} , globally averaged); in fact, comparing the radiative flux imbalance suggests the latent heat flux is actually smaller.
14. To investigate the effect of condensation on the thermal structure [see also J. L. Kasting, *Icarus* **94**, 1 (1991)], we replaced the convective lower region in the atmosphere with one held to the saturation vapor curve. The radiative solution is recomputed, and the layer immediately above the saturated region is tested for saturation. If its temperature is lower than the saturation temperature for that pressure, the forced saturated region is extended one layer upward and the process repeated until convergence is achieved. The atmosphere is 30 layers deep, with layers varying in thickness from about 1 km near the surface, to about 15 km at the top (typically 300 km or so, where the pressure is less than 1 mbar).
15. R. D. Lorenz and J. I. Lunine, *Icarus* **122**, 79 (1996).
16. P. H. Smith *et al.*, *ibid.* **119**, 336 (1996).
17. A. Coustenis, E. Lellouch, J. P. Maillard, C. P. McKay, *ibid.* **118**, 87 (1995); C. A. Griffith, T. Owen, R. Wagener, *ibid.* **93**, 362 (1991); M. T. Lemmon, E. Karkoschka, M. Tomasko, *ibid.* **113**, 27 (1995).
18. D. Morrison, T. Owen, L. A. Soderblom, in *Satellites*, J. Burns and M. S. Matthews, Eds. (Univ. of Arizona Press, Tucson, 1986), pp. 764–801.
19. Advective heat transport is often represented in two-dimensional climate models as a diffusion process, with the diffusion coefficient proportional to pressure (27). The 1 MW m^{-1} heat flux indicated in the text corresponds to a scale height of the present atmosphere with a temperature increment of 10 K moving poleward at 1 cm s^{-1} .

20. On Earth, annually averaged meridional heat transport peaks at mid-latitudes at $\sim 200 \text{ MW m}^{-1}$ of which about a quarter is transported by ocean currents; see, for example, R. McIlveen, *Fundamentals of Weather and Climate* (Chapman & Hall, London, 1992). Titan's probably cratered landscape may prevent large-scale liquid motions [S. F. Dermott and C. Sagan, *Nature* **374**, 238 (1995)], confining

liquids to lakes [R. D. Lorenz, *Planet. Space Sci.* **42**, 1 (1994)].
21. P. J. Gierasch and O. B. Toon, *J. Atmos. Sci.* **30**, 1502 (1973).
22. W. R. Thompson, J. A. Zollweg, D. H. Gabis, *Icarus* **97**, 187 (1992); L. C. Kouvaris and F. M. Flasar, *ibid.* **91**, 112 (1991); J. I. Lunine and D. J. Stevenson, *Nature* **317**, 238 (1985).

23. S. Engel, J. I. Lunine, W. K. Hartmann, *Planet. Space Sci.* **43**, 1059 (1995).
24. R. D. Lorenz, *ibid.* **44**, 1021 (1996).
25. J.I.L. and C.P.M. were supported through the NASA Planetary Atmospheres and Geology-Geophysics programs, and R.D.L. through the Cassini project.

3 September 1996; accepted 18 December 1996

Earth-Based Radio Tracking of the Galileo Probe for Jupiter Wind Estimation

W. M. Folkner, R. A. Preston, J. S. Border, J. Navarro*, W. E. Wilson, M. Oestreich

Although the Galileo probe was designed to communicate only to the orbiter, the probe radio signal was detected at two Earth-based radio observatories where the signal was a billion times weaker. The measured signal frequency was used to derive a vertical profile of the jovian zonal wind speed. Due to the mission geometry, the Earth-based wind estimates are less sensitive to descent trajectory errors than estimates based on probe-orbiter Doppler measurements. The two estimates of wind profiles agree qualitatively; both show high wind speeds at all depths sampled.

On 7 December 1995 the Galileo probe entered the atmosphere of Jupiter. One of the goals of the probe mission was to determine the jovian zonal (east-west) wind speed as a function of altitude by measurements of the Doppler shift of the probe radio signal received by the orbiter. Prior to the Galileo mission, various combinations of Doppler, radio interferometric, and in situ measurements of atmospheric probes from the Pioneer, Venera, and Vega missions have been used to investigate the wind speed on Venus (1). Remote observations of Jupiter's clouds show complex structure and large variation in wind speed (2). The remote observations do not penetrate the upper cloud layers and cannot determine whether the winds are driven by solar energy, which is largely absorbed in the upper cloud layers or by Jupiter's internal energy. Measurements of the Doppler shift of the probe radio signal help estimate the wind speed below the levels where sunlight is absorbed and help determine the driving mechanism.

The Galileo orbiter was nearly directly above the probe throughout the descent to maximize the signal received by the orbiter, and thus the probe-orbiter link was nearly perpendicular to the zonal wind direction. This creates some ambiguity in interpreting

the probe-orbiter Doppler shift, since vertical updrafts and downdrafts or meridional winds could cause Doppler shifts potentially as large as caused by the zonal winds (3). After the Galileo mission was launched, it was realized that the probe radio signal could be directly detected at Earth for at least part of its descent even though the signal power was 10^9 times weaker at Earth than at the orbiter. Because the probe-Earth direction was almost parallel with the zonal wind direction, the Doppler shift as received at Earth was less sensitive to probe descent trajectory modeling than the probe-orbiter measurements (4).

The probe transmitted data to the orbiter on two channels near 1387 MHz (21.6 cm). Probe telemetry was sent at 256 symbols per second on each channel during the entire descent of the probe through the atmosphere with a fully suppressed carrier (5). One of the two probe channels was controlled by an ultra-stable oscillator (USO). This oscillator provided the frequency stability over the descent of the probe necessary to ensure that oscillator drifts were negligible compared with Doppler shifts due to changes in the wind speed. The probe carrier frequency received at the orbiter was compared to the frequency of a similar USO on the orbiter. The differenced frequency data were transmitted to Earth. Through the Doppler effect, these differenced frequency values provided a measure of relative velocity between the probe and the orbiter along the probe-orbiter direction. This velocity measurement did not represent the absolute velocity of the probe in this direction, but rather the sum of probe velocity and a (nearly) constant un-

known bias, with the bias caused by the difference of the unknown frequency offsets of the probe and orbiter oscillators from their nominal frequencies.

The probe antenna pointed vertically, with the orbiter nearly overhead for best reception of the probe telemetry. Earth was near the horizon as seen from the probe. Consequently the antenna gain in the direction toward Earth was low. The power transmitted in the direction of Earth was about 60 times less than the vertical power for the first 3 min of probe transmission. As the probe descended the rotation of Jupiter caused the probe antenna to point farther from Earth so that the power transmitted toward Earth decreased to 200 times less than the vertical power 35 min after probe entry. In addition Earth was about 4000 times farther from the probe than the orbiter was.

During the probe descent, the Very Large Array (VLA) in Socorro, New Mexico, was configured to point at the Galileo probe with the signals from all 27 antennas combined to provide a collecting area equivalent to that of a 130-m diameter radio antenna. The Australia Telescope Compact Array (ATCA) in Narrabri, Australia, was similarly configured as a backup site, with its six antennas combined to form the equivalent of a 54-m diameter antenna. Since the probe signal was 100% phase-modulated by the telemetry stream, real time detection of the probe signal required sufficient signal to noise (SNR) in one symbol-time (~ 4 ms), which could be achieved at the orbiter but not at the Earth-based sites. Instead the Earth-based sites performed a wide band open loop recording of the probe signal for later processing. By using the known probe symbol stream, as relayed by the orbiter to Earth, the phase modulation on the probe signal due to the telemetry could be removed from the open loop recording of the probe signal, which allowed longer coherent integration times. The probe signal was successfully detected at both sites. The stronger VLA signal was used for most of the data reduction and analysis.

After removal of the telemetry modulation, the SNR at the VLA would have been adequate to determine the probe radio frequency with a simple phase-locked-loop algorithm if the signal frequency had been changing slowly enough. However the

W. M. Folkner, R. A. Preston, J. S. Border, Jet Propulsion Laboratory, California Institute of Technology, Pasadena, CA 91109, USA.

J. Navarro, National Radio Astronomy Observatory, Socorro, NM, 87801 USA.

W. E. Wilson and M. Oestreich, CSIRO Australia Telescope National Facility, Epping, New South Wales, Australia.

*Present address: Kvednaberget 12, 4033 Forus, Norway.